






Cite this: *J. Mater. Chem. A*, 2023, **11**, 7193

# Highly tough, degradable, and water-resistant bio-based supramolecular plastics comprised of cellulose and tannic acid†

Haoxiang Sun, Xu Fang, Youliang Zhu,  Zhuochen Yu,  Xingyuan Lu and Junqi Sun \*

It is challenging to fabricate high-performance degradable plastics that simultaneously possess high mechanical strength, satisfactory water resistance and rapid degradation characteristics in natural environments using biomass resources. In this study, mechanically robust, water-resistant, biocompatible, and degradable plastics are fabricated through the complexation of regenerated cellulose and tannic acid (TA) followed by molding these complexes into desired shapes. The resulting plastic (denoted as C-TA) prepared with 15 wt% TA exhibits an ultrahigh fracture strength of  $\sim 265$  MPa and a toughness of  $\sim 55.2$  MJ m<sup>-3</sup>. An all-atom molecular dynamics simulation demonstrates that the introduction of dendritic TA molecules notably enhances the toughness of the C-TA plastic through the formation of TA-centered hydrogen-bond clusters. The C-TA plastic retains a fracture strength of  $\sim 166$  MPa and  $\sim 98$  MPa after being stored in environments with relative humidities of 80% and 100% for 7 days, respectively, indicating its excellent water resistance. The good water resistance and high mechanical strength of the C-TA plastic originate from the hydrophobic aromatic rings of its TA molecules and its TA-centered hydrogen-bond clusters which serve as cross-links and nanofillers to strengthen the plastic. The C-TA plastic can be fully degraded in soil into nontoxic species within 35 days.

Received 19th January 2023  
Accepted 9th March 2023

DOI: 10.1039/d3ta00351e

[rsc.li/materials-a](http://rsc.li/materials-a)

## 1. Introduction

The accumulation of plastic waste in the environment has become a pervasive and growing problem. It is estimated that by 2050, there will be 12 billion tonnes of plastic waste.<sup>1–3</sup> Currently, governments are significantly promoting the usage of degradable plastics to mitigate plastic pollution.<sup>4–8</sup> However, the development of degradable plastics to replace conventional petroleum-based plastics faces bottlenecks due to the high production costs, unsatisfactory mechanical performance and degradability of existing degradable plastics.<sup>9–13</sup> Bio-based degradable plastics, which are (partly) derived from biomass, have recently attracted increasing interest because of their valuable properties such as sustainable resources, high biocompatibility and efficient degradability.<sup>4,6,10,14</sup> Cellulose is one of the most abundant natural polymers and shows great potential for the mass production of bio-based degradable plastics.<sup>15–17</sup> However, cellulose-based plastics are fragile due to the highly ordered nanofiber structure of cellulose.<sup>18</sup> Moreover, the hydrophilic nature of cellulose leads to unsatisfactory water

resistance, which largely limits the applications of cellulose-based plastics. The incorporation of chemical cross-links into cellulose provides an effective strategy to improve its mechanical properties and water resistance.<sup>18,19</sup> For example, Zhang and co-workers developed a highly tough and water-resistant cellulose plastic by chemically cross-linking cellulose with epichlorohydrin followed by pre-stretching to a strain of 40%.<sup>18</sup> The resulting cellulose plastic exhibits a high toughness of  $\sim 41.1$  MJ m<sup>-3</sup> and a fracture strength of  $\sim 148$  MPa. However, chemically cross-linked cellulose plastics usually exhibit reduced degradation rates.<sup>20,21</sup> Alternatively, stiff nanofillers can also be blended into cellulose to improve the water resistance and mechanical properties of cellulose-based plastics.<sup>22–25</sup> Most nanofiller-reinforced cellulose-based plastics exhibit unsatisfactory toughness because of the low interfacial compatibility and weak interactions between the nanofillers and cellulose chains.<sup>25</sup> Therefore, the fabrication of cellulose-based plastics that simultaneously possess high strength and toughness, good water resistance, and rapid and highly efficient degradability in natural environments is still a significant challenge.

Supramolecular plastics can be fabricated by cross-linking prepolymers or (macro)monomers with noncovalent interactions and/or dynamic covalent bonds.<sup>4,5,26–29</sup> The reversible cross-linking of degradable biomass species allows for the fabrication of supramolecular plastics with desirable recyclability and degradability.<sup>4,30,31</sup> Degradable plastics generally

State Key Laboratory of Supramolecular Structure and Materials, College of Chemistry, Jilin University, Changchun 130012, PR China. E-mail: [sun\\_junqi@jlu.edu.cn](mailto:sun_junqi@jlu.edu.cn)

† Electronic supplementary information (ESI) available. See DOI: <https://doi.org/10.1039/d3ta00351e>

exhibit low and inefficient degradation with increasing their mechanical robustness and water resistance. For example, with increasing molecular weight, poly(lactic acid) (PLA) plastics exhibit improved fracture strength and water resistance, but they also show reduced degradation rates.<sup>32–34</sup> Therefore, engineering the types, density and distribution of the dynamic interactions of degradable supramolecular plastics to balance the degradability, robustness and water resistance will be essential. We propose that well-designed hydrogen bonds in degradable supramolecular plastics can be employed to improve the mechanical strength, toughness and water resistance of these plastics while simultaneously achieving efficient degradability. This is because hydrogen bonds can serve as cross-links that can be broken in moist soil. Tannic acid (TA) is a natural dendritic polyphenol molecule with a high density of hydrogen bonding sites that can form strong hydrogen bonds with cellulose.<sup>35–37</sup> Although TA has been used to improve the mechanical strength of polymer composites, TA-based degradable plastics are rarely reported.<sup>38,39</sup> We believe that the complexation of cellulose with TA can generate TA-centered hydrogen bond clusters, which will serve as strong cross-links to efficiently strengthen these cellulose plastics. Meanwhile, the hydrophobic aromatic rings of the TA molecules and the TA-centered hydrogen bond clusters can balance their water resistance and degradability. Following this design principle, we demonstrate the fabrication of a mechanically robust and degradable cellulose-based supramolecular plastic with good water resistance and degradability through the complexation of cellulose and TA. This supramolecular plastic exhibits a high mechanical strength of  $\sim 265$  MPa and toughness of  $\sim 55.2$  MJ  $m^{-3}$ . In an environment with 100% relative humidity (RH), the fracture strength of the cellulose-based plastic is still  $\sim 98$  MPa. This plastic is biocompatible and can autonomously degrade into non-toxic species in soil within  $\sim 35$  days.

## 2. Results and discussion

### 2.1. Synthesis of C-TA plastics

The structures of cellulose and TA are presented in Fig. 1a. As shown in Fig. 1a, the C-TA plastics were fabricated by mixing dimethylacetamide (DMAc) solutions containing cellulose and TA with different mass ratios under continuous stirring at 40 °C. To obtain cellulose solutions, degreasing cotton was first suspended in DMAc in the presence of LiCl for 12 h at 110 °C. After continued stirring for 12 h at room temperature, clear viscous cellulose solution was obtained. The degree of polymerization (DP) of cellulose was measured to be  $\sim 810$ . The DMAc solution containing C-TA complexes (denoted C-TA<sub>x</sub>, where *x* represents the mass ratio of TA to cellulose) was cast onto a glass plate to obtain C-TA<sub>x</sub> organic gel after drying at 40 °C for 12 h. After dialyzing the C-TA<sub>x</sub> organic gel in water followed by drying at room temperature, a piece of transparent and flexible C-TA<sub>x</sub> plastic was obtained. Fig. 1b shows that this C-TA<sub>0.15</sub> plastic is both flexible and highly transparent, with a transmittance of  $\sim 85\%$  at 500 nm (Fig. S1†). The C-TA<sub>x</sub> plastic is mainly cross-linked with three types of hydrogen bonds: (i) those among the hydroxyl groups on cellulose chains; (ii) those between the

hydroxyl groups of cellulose and the phenolic hydroxyl groups of TA molecules; (iii) those between the hydroxyl groups of cellulose and the ester carbonyl or ester ether oxygen groups of TA molecules. The Fourier-transform infrared (FTIR) spectra shown in Fig. S2† demonstrate that the characteristic peak of the hydroxyl groups at  $3417\text{ cm}^{-1}$  in the cellulose film spectrum shifts to  $3407\text{ cm}^{-1}$  in the C-TA<sub>0.15</sub> plastic spectrum. Meanwhile, the characteristic peak of ester carbonyl at  $1703\text{ cm}^{-1}$  in the TA spectrum shifts to  $1728\text{ cm}^{-1}$  in the C-TA<sub>0.15</sub> plastic spectrum. These results confirm the formation of hydrogen bonds between the hydroxyl groups of cellulose and the phenolic hydroxyl groups and ester carbonyl groups of TA. An all-atom molecular dynamics (MD) simulation was conducted to further confirm the formation of the hydrogen bonds between the cellulose chains and TA molecules.<sup>40</sup> As shown in Fig. 1c, dendritic TA molecules with rich hydrogen bond donors and acceptors can bind cellulose chains through hydrogen bonds to form TA-centered hydrogen-bond clusters. A binding energy (BE) calculation was carried out to measure the strength of the hydrogen bonds in the C-TA<sub>0.15</sub> plastic. As shown in Fig. S3a,† the binding energy of hydrogen bonds between the hydroxyl groups of cellulose is  $-18.657\text{ kJ mol}^{-1}$ , which is close to that of hydrogen bonds between the hydroxyl groups of cellulose and the phenolic hydroxyl groups of TA ( $-18.199\text{ kJ mol}^{-1}$ , Fig. S3b†). However, the hydrogen bonds between the hydroxyl groups of cellulose and the ester carbonyl or ester ether oxygen groups of TA exhibit much higher binding energies of  $-28.401\text{ kJ mol}^{-1}$  and  $-28.861\text{ kJ mol}^{-1}$  (Fig. S3c†), respectively. This result suggests that the TA-centered hydrogen bond clusters in C-TA<sub>0.15</sub> plastics are stronger than the hydrogen bonds in the cellulose plastic. X-ray diffraction (XRD) patterns of the cellulose and C-TA<sub>0.15</sub> plastics show clear cellulose II peaks at  $2\theta = 12.5^\circ$  and  $20.0^\circ$ , which are assigned to the cellulose II (110) and (200) planes, respectively.<sup>29,41</sup> This indicates the existence of crystalline cellulose II in the cellulose and C-TA<sub>0.15</sub> plastics (Fig. S4†).

### 2.2. Mechanical properties of C-TA<sub>x</sub> plastics

The mechanical properties of the C-TA<sub>x</sub> plastics were measured by tensile tests at a stretching speed of  $10\text{ mm min}^{-1}$  under the ambient conditions of  $\sim 60\%$  RH and  $25\text{ }^\circ\text{C}$  (Fig. 2a). The mechanical properties (fracture strength, strain at break, Young's modulus, and toughness) of these samples are summarized in Table S1.† The cellulose plastic is highly stiff and brittle, with a high fracture strength of  $\sim 196$  MPa and a strain at break of  $\sim 23.4\%$ . The introduction of TA (mass ratio of TA to cellulose ranging from 0 to 0.15) to prepare C-TA<sub>x</sub> plastics leads to a notable increase in both fracture strength and toughness compared with the cellulose plastic. A decrease in the fracture strength and toughness occurs when the mass ratio of TA to cellulose reaches 0.25, meaning that a higher cross-linking density of the TA-centered hydrogen bond clusters in the C-TA<sub>0.25</sub> plastic makes this plastic more fragile. Among these plastics, the C-TA<sub>0.15</sub> plastic is the mechanically strongest and exhibits a fracture strength of  $\sim 265$  MPa, Young's modulus of  $\sim 7.64$  GPa, strain at break of  $\sim 31.9\%$  and toughness of  $\sim 55.2$

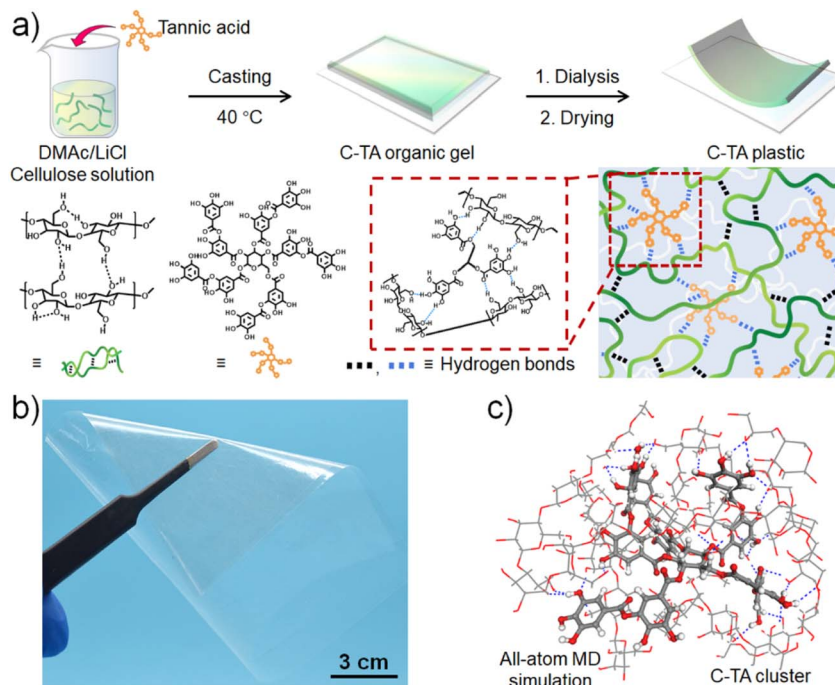


Fig. 1 (a) Schematic of the preparation process for the C-TA plastic and illustration of the proposed hydrogen bonds in C-TA plastic. (b) Digital image of a piece of C-TA<sub>0.15</sub> plastic with a size of 15 cm × 10 cm. The plastic has a thickness of ~50 μm. (c) Snapshot of the all-atom MD simulation of the structure of the TA-centered hydrogen-bond cluster.

MJ m<sup>-3</sup>. These values are 1.35, 1.22, 1.36, and 1.73 times higher than those of the cellulose plastic, respectively. As shown in Fig. 2b, a C-TA<sub>0.15</sub> plastic strip with a width of 5 mm and thickness of 50 μm can hold a 5 kg dumbbell without fracturing. As summarized in Fig. 2c, the fracture strength and toughness of the C-TA<sub>0.15</sub> plastics are high compared with traditional

engineering and cellulose-based plastics reported in literature.<sup>18,22,24,42,43</sup> The high brittleness of cellulose plastics arises from their highly ordered nanofiber structure. The introduction of dendritic TA can break a fraction of the hydrogen bonds between cellulose chains and simultaneously form TA-centered hydrogen bond clusters with cellulose. Therefore, an all-atom

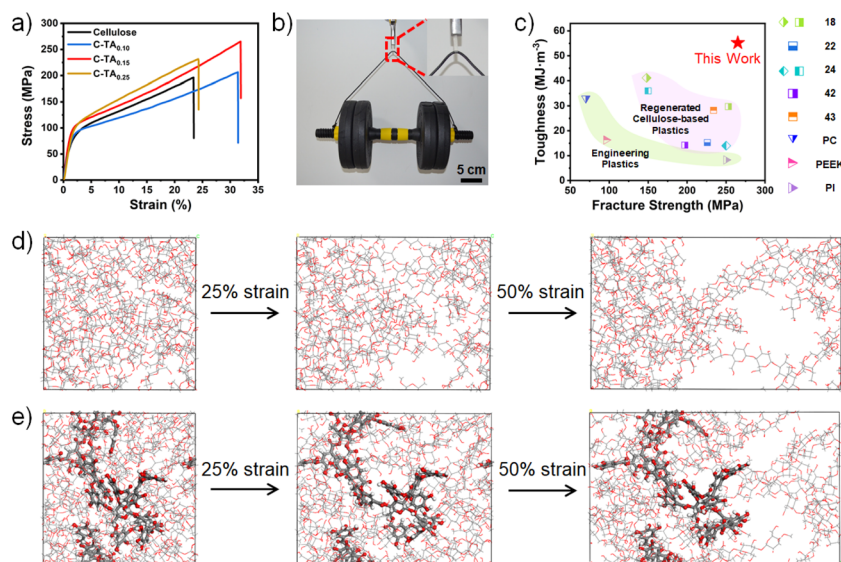


Fig. 2 (a) Stress–strain curves of C-TA<sub>x</sub> plastics with different mass ratio of TA to cellulose. (b) Digital image of a piece of C-TA<sub>0.15</sub> plastic strip that can lift a weight of 5 kg. (c) Comparison of the fracture strength of the C-TA<sub>0.15</sub> plastic and some of the engineering plastics (PC: polycarbonate, PEEK: poly(ether-ether-ketone), PI: polyimide), and regenerated cellulose-based plastics.<sup>18,22,24,42,43</sup> (d, e) Snapshots showing the MD simulations of the cellulose plastic (d) and the C-TA<sub>0.15</sub> plastic (e) before and after being stretched to the strains of 25% and 50%.

tensile simulation was carried out to understand the mechanism of the TA-centered hydrogen bond clusters in enhancing the mechanical properties of the C-TA<sub>0.15</sub> plastic. As shown in Fig. 2d, the distribution of the cellulose molecules in the cellulose plastic is homogeneous in the initial box. A large number of voids are generated during the stretching of the cellulose plastic to 25% strain (Movie S1†). Continuously increasing the strain leads to the extension of these voids, and finally, the cellulose plastic fractures. In contrast, no obvious voids can be observed in the C-TA<sub>0.15</sub> plastic at 25% strain. The appearance of voids is only observed after stretching the C-TA<sub>0.15</sub> plastic to 50% strain (Fig. 2e and Movie S2†). Therefore, compared with cellulose plastic, the C-TA<sub>0.15</sub> plastic exhibits remarkably improved fracture strength and toughness. The enhanced mechanical performance of the C-TA<sub>0.15</sub> plastic can be attributed to the formation of TA-centered hydrogen bond clusters. The high-strength hydrogen bonds between the hydroxyl groups of cellulose and the ester carbonyl or ester ether oxygen groups of TA molecules can serve as strong cross-links to strengthen the C-TA<sub>0.15</sub> plastic, leading to higher mechanical strength than that of cellulose plastic. Moreover, the TA-centered hydrogen-bond clusters can effectively enhance the toughness of the C-TA<sub>0.15</sub> plastic by transmitting and dispersing the local stress. This reduces the stress concentration during the stretching process. As described in a following section, the C-TA<sub>0.15</sub> plastic, which exhibits the highest fracture strength and toughness of the prepared plastics, was investigated for use as a degradable supramolecular plastic.

The C-TA<sub>0.15</sub> plastic can be conveniently welded with the assistance of a DMAc solution containing C-TA<sub>0.15</sub>. To investigate its weldability, a C-TA<sub>0.15</sub> plastic sheet was cut into two halves with a blade. The ends of the two separate halves were immersed in C-TA<sub>0.15</sub> solution, then overlapped and dried at room temperature. This was followed by dialysis in deionized water to remove LiCl. The scanning electron microscopy (SEM) images shown in Fig. S5† indicate that the overlapped surfaces are strongly welded. The stress-strain curve displayed in Fig. S6† shows that the welded C-TA<sub>0.15</sub> plastic exhibits a fracture strength of ~249 MPa and a Young's modulus of ~7.3 GPa. The excellent welding ability of the C-TA<sub>0.15</sub> plastic arises from the breakage and reformation of hydrogen bonds in the presence of the DMAc solution containing C-TA<sub>0.15</sub>.<sup>44</sup> In particular, the solvated LiCl breaks the hydrogen bonds on the surface of the C-TA<sub>0.15</sub> plastic sheets. The hydrogen bonds at the interface between the two C-TA<sub>0.15</sub> plastic sheets are re-formed after removing the solvated LiCl *via* dialysis in deionized water, which enables the welding of the plastics.

### 2.3. Thermal stability and water resistance of C-TA<sub>0.15</sub> plastics

Achieving good thermal stability at high temperatures is important for the application of plastics. Therefore, the thermal stability of the C-TA<sub>0.15</sub> plastics was examined by thermal gravimetric analysis (TGA). As shown in Fig. S7,† the decomposition temperature at 5% weight loss ( $T_d$ ) of the C-TA<sub>0.15</sub> plastic is ~299 °C, indicating good thermal stability. The

temperature-dependent mechanical stability of C-TA<sub>0.15</sub> was investigated by dynamic mechanical analysis (DMA). As shown in Fig. 3a, the storage modulus and loss modulus of the C-TA<sub>0.15</sub> plastic are nearly constant in the temperature range of 25 to 150 °C. Moreover, the C-TA<sub>0.15</sub> plastic exhibits a storage modulus as high as ~3600 MPa at 200 °C. The good thermal stability of the C-TA<sub>0.15</sub> plastic mainly originates from cellulose (Fig. S8†). These results indicate that the C-TA<sub>0.15</sub> plastic possesses satisfactory mechanical stability even at high temperatures.

To investigate water resistance, the cellulose and C-TA<sub>0.15</sub> plastics were stored in environments with 80% or 100% RH at room temperature for 7 days and then subjected to tensile tests. As shown in Fig. 3b and Table S2,† the cellulose plastic exhibits a fracture strength of ~99 MPa and Young's modulus of ~4.62 GPa under the 80% RH environment. These values decrease to ~56 MPa and ~2.64 GPa under the 100% RH environment. In contrast, the C-TA<sub>0.15</sub> plastic has a fracture strength of ~166 MPa and Young's modulus of ~6.67 GPa under the 80% RH environment. Under the 100% RH environment, the fracture strength and Young's modulus of the C-TA<sub>0.15</sub> plastic are ~98 MPa and ~3.20 GPa, respectively. The introduction of TA leads to a significant increase in the fracture strength and Young's modulus under humid environments compared to the TA-free cellulose plastic. The cellulose and C-TA<sub>0.15</sub> plastics have water contact angles of ~87.2° and ~98.2°, respectively. The water resistance of the C-TA<sub>0.15</sub> plastic was further investigated by measuring the water content of the plastics under environments of different RHs. As shown in Fig. S9,† the water content of the C-TA<sub>0.15</sub> plastics is 12.1% under 80% RH and 14.7% under 100% RH. These values are significantly lower than those of cellulose plastic (water content of 29.8% under 80% and 43.7% under 100% RH). Furthermore, as shown in Fig. 3c, after immersion in water for 48 h, the cellulose plastic becomes a soft hydrogel with a fracture strength of ~25 MPa. In contrast, the C-TA<sub>0.15</sub> plastic still maintains a fracture strength of ~34 MPa after immersion in water for 48 h. This performance is comparable to that of high-density polyethylene plastic. Fig. 3d shows that the hydrated C-TA<sub>0.15</sub> plastic (with a thickness of ~50 µm and width of ~10 cm) can hold five weights with a total mass of 2.5 kg underwater without fracture. In water environments, the significantly decreased mechanical strength of the cellulose plastic is caused by the dissociation of hydrogen bonds among the hydroxyl groups on the cellulose chains. In the presence of water, the hydrophobic aromatic rings of TA molecules and the TA-centered hydrogen bond clusters have higher stability than the hydrogen bonds between the hydroxyl groups in the cellulose plastic. This endows the C-TA<sub>0.15</sub> plastics with enhanced water resistance and improved mechanical strength in water environments.

### 2.4. Degradability and biocompatibility of C-TA<sub>0.15</sub> plastics

The degradability of the C-TA<sub>0.15</sub> plastics was investigated by recording the changes in mass as a function of time when buried in soil (Fig. 4a). C-TA<sub>0.15</sub> plastic samples with an area of



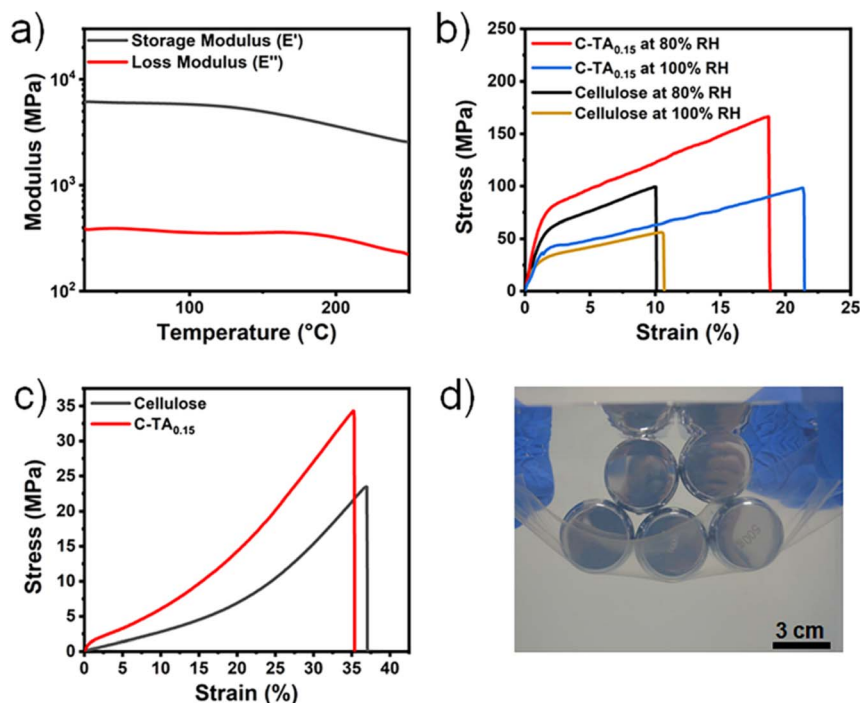


**Fig. 3** (a) DMA curves of C-TA<sub>0.15</sub> plastic. (b) Stress–strain curves of cellulose and C-TA<sub>0.15</sub> plastics after being exposed to environments of 80% and 100% RH at 25 °C for 7 days. (c) Stress–strain curves of cellulose and C-TA<sub>0.15</sub> plastics after being immersed in water for 2 days. (d) Digital image of a C-TA<sub>0.15</sub> plastic sheet that can lift 5 × 500 g weights under water. The plastic sheet has a length of 15 cm, width of 10 cm, and thickness of 50 μm.

2.5 × 2.5 cm<sup>2</sup> and thickness of ~50 μm were buried in soil (Fig. 4b–f), and the change in mass was recorded every 7 days. As shown in Fig. 4a, the mass of the C-TA<sub>0.15</sub> plastic samples slowly decreases in the first 7 days, after which plastic degradation accelerates. The complete degradation of the plastic takes about 35 days. Fig. 4b–f shows the changes in morphology of the C-TA<sub>0.15</sub> plastic buried in soil over time. The plastic buried in soil for 7 days maintains its shape integrity, but its surfaces are stained with microorganisms (Fig. 4c). Plastic degradation occurs from the edges, with eroded holes being observed

(Fig. 4d and e). Finally, the plastic becomes fragmented, and it is completely degraded within ~35 days (Fig. 4f). The all-biomass-derived C-TA<sub>0.15</sub> plastic exhibits fast and highly efficient degradation in soil. This is because the C-TA<sub>0.15</sub> plastic can absorb water, so it becomes swollen when buried in soil. This is accompanied by the partial breakage of hydrogen bonds in the plastic. The enzymes secreted by microorganisms can adhere to the surface of the plastic, eventually penetrating the swollen plastic.<sup>45,46</sup> Some of these enzymes are cellulases secreted by microorganisms, which can effectively cleave the β-1,4-

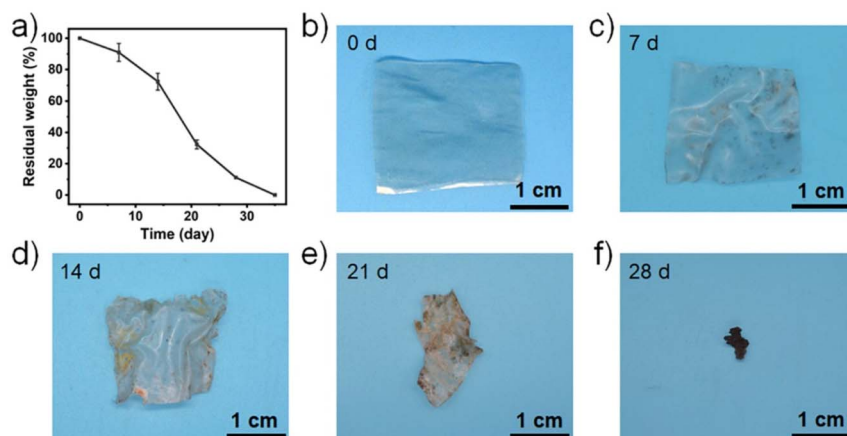


**Fig. 4** (a) Residual weight of the C-TA<sub>0.15</sub> plastics as a function of time in soil. (b–f) Digital images of the intact C-TA<sub>0.15</sub> plastic (b) and the same plastic after being buried in soil for 7 (c), 14 (d), 21 (e), and 28 (f) days.

glucosidic bonds on the cellulose chains. This degrades the cellulose into glucose and finally  $\text{CO}_2$  and  $\text{H}_2\text{O}$ .<sup>47</sup> Meanwhile, tannase, which is mainly produced by fungi (including *aspergillus* and *penicillium* species), can hydrolyze the ester and depside bonds of TA molecules to generate gallic acid and glucose, which are also eventually degraded into  $\text{CO}_2$  and  $\text{H}_2\text{O}$ .<sup>48</sup> In this way, the C-TA<sub>0.15</sub> plastic degrades into  $\text{CO}_2$  and  $\text{H}_2\text{O}$  when buried in soil.

The biocompatibility and non-toxicity of the C-TA<sub>0.15</sub> plastic were characterized by *in vitro* and *in vivo* biocompatibility tests.<sup>4,49,50</sup> For the *in vitro* biocompatibility tests, LO2 cell lines were cultured in 24-well plates in the presence of C-TA<sub>0.15</sub> plastic. After cultivation for 2 and 7 days, the cells were subjected to live/dead assay. As shown in Fig. 5a, all the cells have strong green signals, demonstrating that the LO2 cells have high cell viability after being incubated for 2 and 7 days in the presence of the C-TA<sub>0.15</sub> plastic. Moreover, the cell morphologies of the LO2 cells cultured with the C-TA<sub>0.15</sub> plastic and cellulose plastic do not show any differences. This result confirms that the C-TA<sub>0.15</sub> plastic has excellent cell biocompatibility. For the *in vivo* biocompatibility tests, a C-TA<sub>0.15</sub> plastic sheet was implanted under the ventral skin of a mouse for two weeks. Next, hematology parameters in serum were investigated and compared with those of a control mouse without an implanted plastic sheet. As shown in Fig. 5b, no significant differences were observed between the hematology parameters of the experimental and control groups including the albumin, globulin, alanine transaminase (ALT), blood urea nitrogen (BUN), white blood cell (WBC), red blood cell (RBC), monocyte (MONO) and lymphocyte (LYM) values. Moreover, hematoxylin and eosin (H&E) staining was used to examine the possible toxicity of the C-TA<sub>0.15</sub> plastic to major organs. As shown in Fig. 5c, no lipid droplets, inflammatory responses, or fibrosis were observed on the histological images of the tissues obtained from the experimental mice. These results

demonstrate that the C-TA<sub>0.15</sub> plastic is highly biocompatible and nontoxic. We believe that this nontoxic C-TA<sub>0.15</sub> plastic is potentially applicable in the medical, food, and cosmetics industries.

### 3. Experimental section

#### 3.1. Dissolution of cellulose

Absorbent cotton (20 g) was cut into small pieces and dried at room temperature for 24 h. Next, LiCl (18 g, 0.42 mol) was added to 200 mL (188 g) DMAc, 2.08 g absorbent cotton was then added into the DMAc solution containing LiCl. After stirring at 110 °C for 12 h and then at 25 °C for another 12 h, a colorless transparent cellulose solution was obtained.

#### 3.2. Preparation of the C-TA<sub>x</sub> plastics

The C-TA<sub>0.15</sub> plastic was prepared by the method illustrated in Fig. 1a. Typically, TA powder (0.3 g, 0.36 mmol) was added to 200 mL of cellulose solution, followed by stirring at 40 °C for 6 h. The obtained clear yellowish solution was cast onto a glass plate to obtain an organic gel. Subsequently, the organic gel was immersed in HCl solution (1 M) for 24 h to obtain a transparent hydrogel. This hydrogel was dialyzed in deionized water and then dried at room temperature to obtain the yellowish transparent C-TA<sub>0.15</sub> plastic was obtained. Cellulose plastic and C-TA<sub>x</sub> plastic were also prepared following the same procedure.

#### 3.3. All-atom molecular dynamics simulations

For the cellulose plastic, the all-atom molecular dynamics simulation system consisted of four cellulose chains. For the C-TA<sub>0.15</sub> plastic, the simulation system consisted of four cellulose chains and two TA molecules. The length of the cellulose chain was 32 repeated units. The simulations were carried out using the Forcite module of Materials Studio (Accelrys Inc., San Diego)

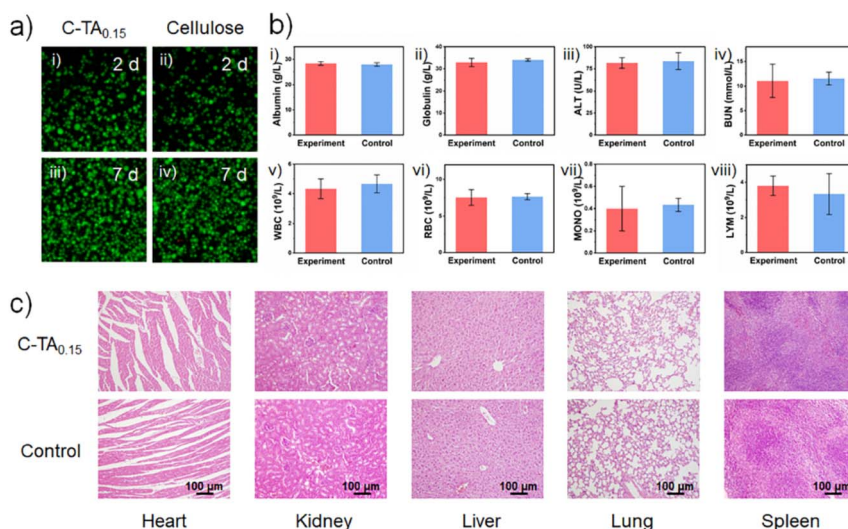


Fig. 5 (a) Live/dead staining of LO2 cells after being cultured on C-TA<sub>0.15</sub> and cellulose plastics for 2 and 7 days. (b) The blood biochemical parameters of the control and experimental mice for the *in vivo* biocompatibility tests. (c) Representative images of the hematoxylin- and eosin-stained heart, kidney, liver, lung, and spleen from the experimental and control mice for the *in vivo* biocompatibility tests.

with a COMPASSII force field. The initial configuration of the simulation systems was constructed by random distribution of molecules using the Amorphous Cell module of Materials Studio. The equilibrium structures were obtained after four annealing cycles, and each cycle included a linear heating process from 300 K to 800 K and a linear cooling process from 800 K to 300 K. The total simulation time was 20 ns under an NPT ensemble at a pressure of 1 bar. The number of hydrogen bonds was counted by recognizing the hydrogen bonding interactions between the hydrogen atom of O–H and an oxygen atom. In this work, the length of the H–O bond was smaller than 2.5 Å and the angle of O–H–O was greater than 150 degrees. Tensile tests were carried out by Geometry Optimization in the Forcite module with 0.5% strain per frame and 100 frames to 50.0% strain.

### 3.4. Biocompatibility tests

The details are provided in ESI.†

## 4. Conclusions

In summary, we demonstrated the fabrication of fully bio-based C-TA<sub>0.15</sub> plastics with excellent mechanical robustness and degradability in soil prepared *via* the complexation of resource-abundant TA and cellulose. Benefiting from its TA-centered hydrogen bond clusters, the C-TA<sub>0.15</sub> plastic exhibits a fracture strength, strain at break, Young's modulus, and toughness of 265 MPa, 31.9%, 7.64 GPa, and 55.2 MJ m<sup>−3</sup>, respectively. The hydrophobic aromatic rings of the TA molecules and the strong hydrogen bond clusters between the TA and cellulose provide the C-TA<sub>0.15</sub> plastic with mechanical robustness comparable to that of high-density polyethylene plastic in water. The C-TA<sub>0.15</sub> plastic exhibits satisfactory thermal stability below 150 °C, ensuring its application in a wide range of temperatures. Furthermore, the bio-based C-TA<sub>0.15</sub> plastic is biocompatible and can be completely and rapidly degraded into nontoxic molecules after being buried in soil for ~35 days. The C-TA<sub>0.15</sub> plastic is composed of resource-abundant and environmentally friendly biomass, and fabricating and processing this plastic is easy. Therefore, this plastic shows good promise for low-cost scalable production. C-TA<sub>0.15</sub> plastics show good potential as substitutes for petroleum-based degradable plastics. We believe that the present work will pave the way for the fabrication of biodegradable supramolecular plastics combining high mechanical strength, good stability, rapid degradation and excellent bio-compatibility for a wide range of practical applications.

## Conflicts of interest

There are no conflicts to declare.

## Acknowledgements

This work was supported by the National Natural Science Foundation of China (NSFC grant 21935004). We thank Prof. Fei

Yan for assistance in characterizing the biocompatibility of the C-TA<sub>0.15</sub> plastics.

## Notes and references

- 1 S. Kakadellis and G. Rosetto, *Science*, 2021, **373**, 49–50.
- 2 W. W. Y. Lau, Y. Shiran, R. M. Bailey, E. Cook, M. R. Stuchtey, J. Koskella, C. A. Velis, L. Godfrey, J. Boucher, M. B. Murphy, R. C. Thompson, E. Jankowska, A. Castillo Castillo, T. D. Pilditch, B. Dixon, L. Koerselman, E. Kosior, E. Favoino, J. Gutberlet, S. Baulch, M. E. Atreya, D. Fischer, K. K. He, M. M. Petit, U. R. Sumaila, E. Neil, M. V. Bernhofen, K. Lawrence and J. E. Palardy, *Science*, 2020, **369**, 1455–1461.
- 3 H. T. H. Nguyen, P. Qi, M. Rostagno, A. Feteiha and S. A. Miller, *J. Mater. Chem. A*, 2018, **6**, 9298–9331.
- 4 X. Fang, N. Tian, W. Hu, Y. Qing, H. Wang, X. Gao, Y. Qin and J. Sun, *Adv. Funct. Mater.*, 2022, **32**, 2208623.
- 5 H. Liu, W. Wei, L. Zhang, J. Xiao, J. Pan, Q. Wu, S. Ma, H. Dong, L. Yu, W. Yang, D. Wei, H. Ouyang and Y. Liu, *Adv. Funct. Mater.*, 2021, **31**, 2104088.
- 6 B. Wang, S. Ma, Q. Li, H. Zhang, J. Liu, R. Wang, Z. Chen, X. Xu, S. Wang, N. Lu, Y. Liu, S. Yan and J. Zhu, *Green Chem.*, 2020, **22**, 1275–1290.
- 7 D.-H. Li, Z.-M. Han, Q. He, K.-P. Yang, W.-B. Sun, H.-C. Liu, Y.-X. Zhao, Z.-X. Liu, C.-N.-Y. Zong, H.-B. Yang, Q.-F. Guan and S.-H. Yu, *Adv. Mater.*, 2023, **35**, 2208098.
- 8 H. J. Kim, Y. Reddi, C. J. Cramer, M. A. Hillmyer and C. J. Ellison, *ACS Macro Lett.*, 2020, **9**, 96–102.
- 9 X. Hou, S. Liu and C. He, *J. Mater. Chem. A*, 2022, **10**, 1497–1505.
- 10 B. Jiang, C. Chen, Z. Liang, S. He, Y. Kuang, J. Song, R. Mi, G. Chen, M. Jiao and L. Hu, *Adv. Funct. Mater.*, 2020, **30**, 1906307.
- 11 T. P. Haider, C. Völker, J. Kramm, K. Landfester and F. R. Wurm, *Angew. Chem., Int. Ed.*, 2019, **58**, 50–62.
- 12 Z.-M. Han, D.-H. Li, H.-B. Yang, Y.-X. Zhao, C.-H. Yin, K.-P. Yang, H.-C. Liu, W.-B. Sun, Z.-C. Ling, Q.-F. Guan and S.-H. Yu, *Adv. Funct. Mater.*, 2022, **32**, 2202221.
- 13 H.-B. Yang, Z.-X. Liu, C.-H. Yin, Z.-M. Han, Q.-F. Guan, Y.-X. Zhao, Z.-C. Ling, H.-C. Liu, K.-P. Yang, W.-B. Sun and S.-H. Yu, *Adv. Funct. Mater.*, 2022, **32**, 2111713.
- 14 X. Wang, Q. Xia, S. Jing, C. Li, Q. Chen, B. Chen, Z. Pang, B. Jiang, W. Gan, G. Chen, M. Cui, L. Hu and T. Li, *Small*, 2021, **17**, 2008011.
- 15 X. Zhang, J. You, J. Zhang, C. Yin, Y. Wang, R. Li and J. Zhang, *CCS Chem.*, 2022, DOI: [10.31635/ccschem.022.20220388](https://doi.org/10.31635/ccschem.022.20220388).
- 16 S. S. A. Athukoralalage, C. A. Bell, A. C. Gemmell, A. E. Rowan and N. Amiralian, *J. Mater. Chem. A*, 2023, **11**, 1575–1592.
- 17 C. M. Clarkson, S. M. El Awad Azrak, E. S. Forti, G. T. Schueneman, R. J. Moon and J. P. Youngblood, *Adv. Mater.*, 2021, **33**, 2000718.
- 18 D. Ye, X. Lei, T. Li, Q. Cheng, C. Chang, L. Hu and L. Zhang, *ACS Nano*, 2019, **13**, 4843–4853.
- 19 X. Zhang, Y. Cheng, J. You, J. Zhang, C. Yin and J. Zhang, *Nat. Commun.*, 2022, **13**, 1117.

- 20 L. Hu, Y. Zhong, S. Wu, P. Wei, J. Huang, D. Xu, L. Zhang, Q. Ye and J. Cai, *Chem. Eng. J.*, 2021, **417**, 129229.
- 21 E. Abraham, P. A. Elbi, B. Deepa, P. Jyotishkumar, L. A. Pothan, S. S. Narine and S. Thomas, *Polym. Degrad. Stab.*, 2012, **97**, 2378–2387.
- 22 H. Tu, K. Xie, X. Lin, R. Zhang, F. Chen, Q. Fu, B. Duan and L. Zhang, *J. Mater. Chem. A*, 2021, **9**, 10304–10315.
- 23 H. Mianehrow, G. Lo Re, F. Carosio, A. Fina, P. T. Larsson, P. Chen and L. A. Berglund, *J. Mater. Chem. A*, 2020, **8**, 17608–17620.
- 24 K. Yu and M.-E. Aubin-Tam, *ACS Appl. Nano Mater.*, 2020, **3**, 12055–12063.
- 25 X. Che, M. Wu, G. Yu, C. Liu, H. Xu, B. Li and C. Li, *Chem. Eng. J.*, 2022, **433**, 133672.
- 26 Z. Zou, C. Zhu, Y. Li, X. Lei, W. Zhang and J. Xiao, *Sci. Adv.*, 2018, **4**, eaaq0508.
- 27 B. Qin, S. Zhang, P. Sun, B. Tang, Z. Yin, X. Cao, Q. Chen, J.-F. Xu and X. Zhang, *Adv. Mater.*, 2020, **32**, 2000096.
- 28 X. Lu, Y. Luo, Y. Li, C. Bao, X. Wang, N. An, G. Wang and J. Sun, *CCS Chem.*, 2020, **2**, 524–532.
- 29 K. Gong, L. Hou and P. Wu, *Adv. Mater.*, 2022, **34**, 2201065.
- 30 P. Sun, S. Wang, Z. Huang, L. Zhang, F. Dong, X. Xu and H. Liu, *Green Chem.*, 2022, **24**, 7519–7530.
- 31 Q. Xia, C. Chen, Y. Yao, J. Li, S. He, Y. Zhou, T. Li, X. Pan, Y. Yao and L. Hu, *Nat. Sustain.*, 2021, **4**, 627–635.
- 32 K.-L. G. Ho, A. L. Pometto and P. N. Hinz, *J. Environ. Polym. Degrad.*, 1999, **7**, 83–92.
- 33 P. Sangwan and D. Y. Wu, *Macromol. Biosci.*, 2008, **8**, 304–315.
- 34 X. Pang, X. Zhuang, Z. Tang and X. Chen, *Biotechnol. J.*, 2010, **5**, 1125–1136.
- 35 H. Fan, J. Wang and Z. Jin, *Macromolecules*, 2018, **51**, 1696–1705.
- 36 S. Yang, Y. Zhang, T. Wang, W. Sun and Z. Tong, *ACS Appl. Mater. Interfaces*, 2020, **12**, 46701–46709.
- 37 Z. Bai, K. Jia, C. Liu, L. Wang, G. Lin, Y. Huang, S. Liu and X. Liu, *Adv. Funct. Mater.*, 2021, **31**, 2104701.
- 38 S. Roy, L. Zhai, H. Kim, D. Pham, H. Alrobei and J. Kim, *Polymers*, 2021, **13**, 228.
- 39 B. Kaczmarek, A. Owczarek, K. Nadolna and A. Sionkowska, *Mater. Lett.*, 2019, **245**, 22.
- 40 A.-T. Kuo, A. Tanaka, J. Irisawa, W. Shinoda and S. Okazaki, *J. Phys. Chem. C*, 2017, **121**, 21374–21382.
- 41 D. Zhao, J. Huang, Y. Zhong, K. Li, L. Zhang and J. Cai, *Adv. Funct. Mater.*, 2016, **26**, 6279.
- 42 T. Zhang, X. Zhang, Y. Chen, Y. Duan and J. Zhang, *ACS Sustainable Chem. Eng.*, 2018, **6**, 1271–1278.
- 43 P. Wei, J. Huang, Y. Lu, Y. Zhong, Y. Men, L. Zhang and J. Cai, *ACS Sustainable Chem. Eng.*, 2019, **7**, 1707–1717.
- 44 C. Zhang, R. Liu, J. Xiang, H. Kang, Z. Liu and Y. Huang, *J. Phys. Chem. B*, 2014, **118**, 9507–9514.
- 45 D. B. Wilson, *Curr. Opin. Microbiol.*, 2011, **14**, 259–263.
- 46 U. Bornscheuer, K. Buchholz and J. Seibel, *Angew. Chem., Int. Ed.*, 2014, **53**, 10876–10893.
- 47 J. Sandhya and R. Renuka, in *Cellulose*, ed. P. Alejandro Rodríguez and E. E. M. María, IntechOpen, Rijeka, 2019, p. Ch. 5, DOI: DOI: [10.5772/intechopen.84531](https://doi.org/10.5772/intechopen.84531).
- 48 L. Mingshu, Y. Kai, H. Qiang and J. Dongying, *J. Basic Microbiol.*, 2006, **46**, 68–84.
- 49 S. Azevedo, A. M. S. Costa, A. Andersen, I. S. Choi, H. Birkedal and J. F. Mano, *Adv. Mater.*, 2017, **29**, 1700759.
- 50 N. Tang, R. Zhang, Y. Zheng, J. Wang, M. Khatib, X. Jiang, C. Zhou, R. Omar, W. Saliba, W. Wu, M. Yuan, D. Cui and H. Haick, *Adv. Mater.*, 2022, **34**, 2106842.